Eur. Phys. J. C 5, 651–664 (1998)
DOI 10.1007/s100529800987

THE EUROPEAN PHYSICAL JOURNAL C

Experimental study of the dynamic Newtonian field with a cryogenic gravitational wave antenna

P. Astone[2], M. Bassan[3,4], R. Bizzarri[1,2], P. Bonifazi[2,6], L. Brocco[1,2], P. Carelli[7,8], E. Coccia[3,4], C. Cosmelli[1,2], A. Degasperis[1,2], S. Frasca[1,2], V. Fafone[5], E. Majorana[2], I. Modena[3,4], G. Modestino[5], A. Moleti[3,4], G.V. Pallottino[1,2], G. Pizzella[3,6], P. Puppo[1,5], P. Rapagnani[1,2], F. Ricci[1,2], R. Terenzi[4,6], M. Visco[4,6]

[1] Dipartimento di Fisica, Università La Sapienza, Roma, Italy
[2] I.N.F.N., Sezione di Roma 1, Roma, Italy
[3] Dipartimento di Fisica, Università Tor Vergata, Roma, Italy
[4] I.N.F.N., Sezione di Roma 2, Roma, Italy
[5] I.N.F.N., Laboratori Nazionali di Frascati, Frascati, Italy
[6] C.N.R., Istituto di Fisica dello Spazio Interplanetario, Roma, Italy
[7] Dipartimento di Energetica, Università de L'Aquila, L'Aquila, Italy
[8] I.N.F.N., Gruppo Collegato de L'Aquila, L'Aquila, Italy

Received: 14 June 1998 / Published online: 16 September 1998

Abstract. We present an experiment performed to study the behaviour of the dynamic gravitational interaction at laboratory scale. We used as field generator a mass quadrupole rotating in the range of 460 Hz and we detected the acceleration field with the cryogenic gravitational wave antenna Explorer of the Rome group. We report the measurements of this interaction as a function of the distance between the field source and the detector. An upper limit on the parameters of a Yukawa-like potential, modeling an hypotetic deviation from the Newtonian law of gravity, is derived.

1 Introduction

Precise measurements of weak effects play a crucial role in metrology and in the determination of the fundamental constants. In this contest the search for deviation from the Newtonian potential has produced remarkable improvements in the knowledge of the fundamental constant G in a wide range of distances, and impressive advances of the measurement techniques. The hypothesis of a possible deviation from the inverse square distance law has focused the attention of the international scientific community, also in view of the fact that gravitation itself is, among all the fundamental interactions, the least understood [1] [2].

Possible deviations from the $1/r^2$ behaviour of the point-like mass interaction can be described by an additional Yukawa-like potential $V_Y(r)$:

$$V_Y(r) = -\alpha G \frac{M_1 M_2}{r} e^{-r/\lambda} \tag{1}$$

where the λ parameter represents the typical interaction distance, and the dimensionless parameter α determines the strength of the resulting force, that is attractive if $\alpha > 0$ [3]. About the nature of this deviation various hypotheses have been suggested, that fall in two broad categories: the deviation is either a function of the chemical composition of the interacting bodies or it is independent of it. In the second case we call it a gravitational deviation, while in the first case it is more correct to talk about a new, non-gravitational force, and the α constant turns out to be a function of the baryonic number and the atomic mass of two interacting bodies [4].

Nearly all experiments currently under way measure an acceleration (or a force) expressed as the gradient of the sum of the newtonian potential and of the hypothetic Yukawian potential [1], obtaining:

$$\mathbf{F} = -G(r) \frac{M_1 M_2}{r^3} \mathbf{r} \tag{2}$$

with

$$G(r) = G_\infty \left[1 + \alpha \left(1 + \frac{r}{\lambda} e^{-r/\lambda}\right)\right] \tag{3}$$

It follows, from the above equation, that any deviation of $G(r)$ from the constant value

$$G_0 = (6.67259 \pm 0.00085)\ 10^{-11}\ N\ m^2\ kg^{-2} \tag{4}$$

leads to a breakdown of the usual $\frac{1}{r^2}$ Newtonian behaviour of the gravitational interaction between two point-like masses.

We recall that among the physical constants G is the least precisely known: all other constants are known better than $1 \cdot 10^{-6}$, while the best value of G [5] has an uncertainty of about $130 \cdot 10^{-6}$. Astronomical data have provided confirmation that, in the weak field limit and

for interplanetary distances, the Newtonian law of gravitation is obeyed with high accuracy [6,7]. Thus, although the product of G by the mass M of an astronomical body may be determined with a precision of 10^{-6}, since the knowledge of the mass M is affected by a large error, it is possible that noticeable differences exist between G measured at astronomical distances and G in the laboratory [8].

To detect the presence of a new force the most widely used instruments are torsion balances, like that employed by Eötvös in his experiment [9] [10].

Instead, the tests of the $\frac{1}{r^2}$ law at laboratory distances (from 1 m to 10^3 m) have been mostly based on the study of the variation of g with altitude, both in deep boreholes [11] [12] and in high towers [13,14]. These experiments led to a better understanding of the relevance of the local topography in the estimation of the free air gradient, but showed no compelling evidence for deviations from the $1/r$ dependence of the potential [15].

Tests of the distance dependence of the gravitational force have also been performed using generators of time-varying gravitational field and mass quadrupole antennas (such as those developed for the search of gravitational waves) as detectors. With this method the ambiguities due to the influence of the surrounding mass distribution are completely eliminated.

The first attempt was done in 1968 by J. Sinsky at the University of Maryland [16]. A dynamic gravitational field was generated by vibrating a cylinder of about 100 kg at 1600 Hz at distances of the order of two meters from the room temperature gravitational wave antenna of J. Weber. He observed an increase of the vibration energy of the order of 20% above the Brownian noise level of the detector.

Starting from 1980, the gravitational wave group of the University of Tokyo carried on several experiments with room temperature antennas to measure the effect of the dynamic gravitational field generated by a rotating quadrupole source [17,18]. These experiments were done in a frequency range below 100 Hz, covering a distance range from 0.1 m to 10 m. The accuracy of this kind of experiment is limited by the antenna brownian motion whose contribution was decreased with a long integration time. Assuming for the gravitational force the form $\frac{1}{r^{2+\delta}}$, they obtained for the δ parameter the values $\delta = (2.1 \pm 6.2) \cdot 10^{-3}$ in the range $(2.6 \div 10.7)$ m, while for the range $(0.1 \div 0.3)$ m they found $\delta = (-0.7 \pm 2.9) \cdot 10^{-3}$.

A similar experiment was performed by the gravitational wave group of the Roma University using the cryogenic gravitational wave antenna of 2270 kg and 916 Hz resonance frequency installed at CERN in Geneva [19] [20]. The main goal of the experiment was to perform an absolute calibration of the gravitational detector [21]. This antenna, equipped with a resonant capacitive transducer and a d.c. SQUID amplifier, operated at 2 K reaching in 1989 the goal of a noise temperature of 5 mK for short burst detection. With this sophisticated detector the Roma group conceived other experiments. One aimed at detecting possible deviations from the $1/r$ dependence of the Newtonian potential by measuring the antenna signal due to a dynamical gravitational near field generated by a rotor with a high quadrupole moment, put at various distances from the detector. This approach should be considered as preliminary to a second experiment, i.e. a null experiment aimed at measuring the field gradient along the antenna due to a rotating baryonic dipole, a nearly symmetric rotor made by suitable materials, which makes the antenna only sensitive to the composition dependent interaction.

In this paper we present the results obtained by performing the $1/r$ experiment. In Sects. 2 and 3 we analyse the source-detector interaction, in Sects. 4 and 5 we give a schematic description of the rotor and the detector, and we describe the detector response to the dynamic field, in Sect. 6 we discuss the systematic effects that limit the experiment accuracy, and in Sect. 7 we report the results obtained with our experimental apparatus. Finally, in Sects. 8 and 9, we analyze these data and we derive the upper limit curve of the coupling parameter α versus the interaction distance λ.

2 The evaluation of the dynamical gravitational signal

Here and in the following section we compute the oscillation amplitude of the antenna, which is an aluminium right cylinder, induced by a gravitational generator, i.e. an object, of suitable shape as to provide a non zero mass quadrupole, which rotates with angular frequency ω, corresponding to half the resonance frequency of the aluminium bar. The motion of the cylinder is analysed in terms of its normal modes, and, in particular, the first longitudinal vibrational mode is considered. In order to simplify the computation we neglect here the perturbation induced by the transducer (see Sect. 3) on the spatial distribution of the vibrational mode; a corrective term representing the direct gravitational excitation of the transducer will be introduced later.

Let us set the origin of the cartesian coordinate system at the center of the bar, a cylinder of radius R and length L.

The acceleration field $\mathbf{a}(\mathbf{x}, t)$ produced by the generator at the $\mathbf{x} = (x_1, x_2, x_3)$ point of the detector, according to (2) and (3), is:

$$\mathbf{a}(\mathbf{x}, t) = G_0 \nabla_x \int d\mathbf{y}\ \rho(\mathbf{y}, t)[\Phi(\mathbf{x} - \mathbf{y}) + \alpha\Psi(\mathbf{x} - \mathbf{y})] \quad (5)$$

where $\rho(\mathbf{y}, t)$ is the density function of the field generator,

$$\Phi(\mathbf{x}) = \mid \mathbf{x} \mid^{-1}$$

and

$$\Psi(\mathbf{x}) = \mid \mathbf{x} \mid^{-1}\ e^{-|\mathbf{x}|/\lambda}$$

is the non-newtonian term. To eliminate the time dependence of function generator density, due to the rotation around own axis, we perform the coordinates change:

$$\mathbf{y} = \delta\hat{u} + R(t)\boldsymbol{\xi} \quad (6)$$

$\delta\hat{u}$ is the position vector ($\mid \hat{u} \mid \; = \; 1$) of a point of the generator lying on the rotation axis $\hat{n}$, at a distance δ from the centre, $\boldsymbol{\xi}$ is the new integration variable, and $R(t)$ is the rotation matrix defined as follows:

$$R(t)\boldsymbol{\xi} = \xi_0\hat{n} + \xi_+\hat{n}_+e^{i\omega t} + \xi_-\hat{n}_-e^{-i\omega t} \tag{7}$$

with

$$\begin{aligned} \xi_0 &= \hat{n}\cdot\boldsymbol{\xi} \\ \xi_\pm &= \frac{1}{\sqrt{2}}(\xi_1 \pm i\xi_2) \\ \xi_1 &= \hat{n}_1\cdot\boldsymbol{\xi} \\ \xi_2 &= \hat{n}_2\cdot\boldsymbol{\xi} \end{aligned} \tag{8}$$

$$\hat{n}_\pm = \frac{1}{\sqrt{2}}(\hat{n}_1 \mp i\hat{n}_2) \tag{9}$$

where $\hat{n}_1$ and $\hat{n}_2$ and the rotation axis $\hat{n}$ form an orthogonal Cartesian frame.

With the new variable the density $\rho(\mathbf{x},t)$ becomes a time independent function, $\rho(\boldsymbol{\xi})$, and the integral expression (5) takes the more explicit form:

$$\begin{aligned} \mathbf{a}(\mathbf{x},t) = G_0\nabla_x \int_{generator} d\boldsymbol{\xi}\ \rho(\boldsymbol{\xi}) \\ \cdot[\Phi(\mathbf{x}-\delta\hat{u}-R(t)\boldsymbol{\xi}) + \alpha\Psi(\mathbf{x}-\delta\hat{u}-R(t)\boldsymbol{\xi}] \end{aligned} \tag{10}$$

We now consider the motion of the elastic cylinder due to the acceleration field. A normal mode with angular frequency ω_0 and displacement field given by the eigenfunction $\mathbf{v}(\mathbf{x})$ has amplitude $q(t)$ which satisfies the following differential equation:

$$\ddot{q}(t) + \frac{\omega_0}{Q_0}\dot{q}(t) + \omega_0^2 q(t) = g(t) \tag{11}$$

where

$$g(t) = \frac{\int_{antenna} d\mathbf{x}\ \mathbf{v}(\mathbf{x})\cdot\mathbf{a}(\mathbf{x},t)}{\int_{antenna} d\mathbf{x}\ \mathbf{v}(\mathbf{x})\cdot\mathbf{v}(\mathbf{x})} \tag{12}$$

and the parameter Q_o accounts for the losses. We are interested in the effect of the field on the first longitudinal vibrational mode of the antenna, whose displacement field $\mathbf{v}(x)$ has the approximate expression:

$$\mathbf{v}(\mathbf{x}) = \left(0, 0, \sin\frac{\pi x_3}{L}\right) \tag{13}$$

This unidimensional approximation is justified by the low radius-length ratio of the aluminium bar $\left(\frac{R}{L} \simeq 0.1\right)$. We note also that the corresponding approximate eigenfrequency $\omega_0 = \pi v_s/L$, where v_s is the sound velocity, is very close to the measured value. Under this assumption the normalization factor of the formula (12) is:

$$N = \int_{antenna} d\mathbf{x}\ \mathbf{v}(\mathbf{x})\cdot\mathbf{v}(\mathbf{x}) = \frac{\pi R^2 L}{2} \tag{14}$$

To compute the integral that appears on the numerator of (12) we perform a multipole expansion of the acceleration field (11). To this aim we use the inequality:

$$\mid \boldsymbol{\xi} \mid < \mid \mathbf{x} - \delta\hat{u} \mid \tag{15}$$

which certainly holds since the linear dimension of the generator is smaller than the distance of the generator to the nearest point of the detector.

This expansion yield a power series representation of the acceleration $\mathbf{a}(\mathbf{x},t)$ with respect to the variable $R(t)\boldsymbol{\xi}$. Because of the time dependence of the vector $R(t)\boldsymbol{\xi}$, see (7), each term of the power expansion is a linear combination of terms oscillating with angular frequencies 0, ω, 2ω, ..., where ω is the angular frequency of the generator.

Since the generator, rotating at ω, produces an excitation at 2ω, the lowest term of the expansion comes from the quadrupole moment of the generator, and this yields for the forcing term $g(t)$ the expression:

$$\begin{aligned} g(t) = \frac{1}{N}G_0\left\{\left[\gamma_N e^{2i\omega t} + \gamma_N^* e^{-2i\omega t}\right]\right. \\ \left. + \left[\gamma_Y e^{2i\omega t} + \gamma_Y^* e^{-2i\omega t}\right]\right\} \end{aligned} \tag{16}$$

where

$$\gamma_N = \frac{3}{2}F_N M_q \tag{17}$$

$$\gamma_Y = \frac{3}{2}\alpha F_Y M_q \tag{18}$$

M_q is the quadrupole moment of the rotor defined as:

$$M_q = \frac{1}{2}\int_{generator} d\boldsymbol{\xi}\ \rho(\boldsymbol{\xi})(\xi_1 + i\xi_2)^2$$

Because of the geometric symmetry of the rotating body, it is easy to realize that M_q can be also expressed as one half of the difference between the two principal inertial momenta of the body along the ξ_1 and ξ_2 axes.

F_N and F_Y are respectively the Newtonian and Yukawian quadrupole terms. These are two integrals computed on the detector volume, and they depend both on the distance δ between the antenna and the generator and on the orientation of the $\hat{u}$ versor, i.e. they depend on the position of the rotor with respect to the detector. In our present experimental configuration (unlike that reported in [21]) $\hat{u}$ is orthogonal both to the rotation axis $\hat{n}$ of the generator and to the cylinder axis x_3 (Fig. 1), i.e.

$$\begin{aligned} \hat{u}_2 &= \hat{x}_2 \\ \hat{u}_1 &= \hat{u}_3 = 0 \end{aligned} \tag{19}$$

Under these conditions F_N and F_Y are given by the following integrals:

$$\begin{aligned} F_N = \frac{1}{2}\int_{antenna} d\mathbf{v}(\mathbf{x})\ \mathbf{v}(\mathbf{x}) \\ \cdot\nabla_x\left(\frac{[x_2-\delta-ix_3]^2}{[x_1^2+(x_2-\delta)^2+x_3^2]^{5/2}}\right) \end{aligned} \tag{20}$$

$$F_Y = \int_{antenna} d\mathbf{x}\ \mathbf{v}(\mathbf{x})\cdot\nabla_x S(\mathbf{x})\ e^{-\frac{|\mathbf{x}-\delta\hat{u}|}{\lambda}} \tag{21}$$

with

$$S(\mathbf{x}) = \frac{[x_2-\delta-iz]^2}{[x_1^2+(x_2-\delta)^2+x_3^2]^{5/2}}$$

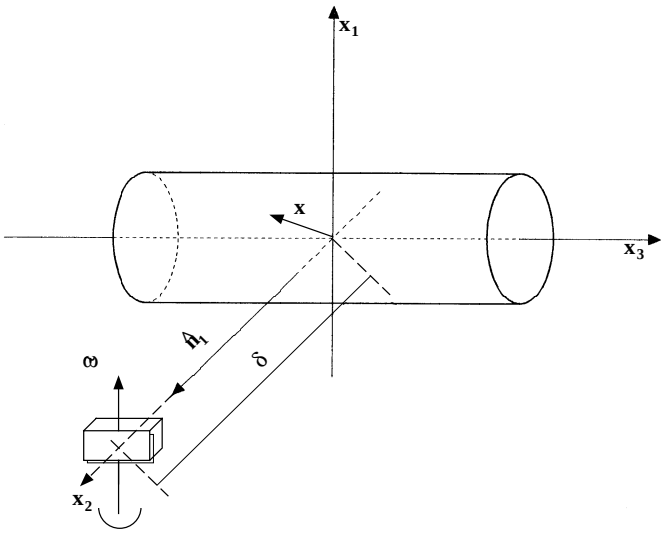

Fig. 1. Model of the rotor-antenna system. $\tilde{\omega}$ is the angular frequency of the rotor and δ the distance between the rotor and the center of mass of the detector

$$\cdot\left(1+\frac{1}{\lambda[x_1^2+(x_2-\delta)^2+x_3^2]^2}+\frac{1}{3\lambda[x_1^2+(x_2-\delta)^2+x_3^2]^{3/2}}\right) \quad (22)$$

F_N and F_Y have been evaluated numerically for each specific value both of the distance δ chosen during the experiment and of the parameter λ considered in the analysis of the data.

3 The detector output

The gravitational wave antenna of the Rome group (Explorer), installed at CERN, is equipped with a resonant capacitive transducer [20]. The resonant transducer can be modelled as an oscillator with frequency ν_t and reduced mass m_t that is coupled to the bar which, in its first longitudinal mode, has frequency ν_b and reduced mass m_b. Since ν_t is tuned within few hertz of ν_b, the transducer and the bar make a system of two coupled oscillators. The equations of motion for the two oscillators are:

$$\begin{cases}\ddot{x}+\frac{\omega_b}{Q_b}\dot{x}+\omega_b^2 x+\mu\frac{\omega_t}{Q_t}(\dot{x}-\dot{y})+\mu\omega_t^2(x-y)=\frac{f_b}{m_b}\\ \ddot{y}+\frac{\omega_t}{Q_t}(\dot{y}-\dot{x})+\omega_t^2(y-x)=\frac{f_t}{m_t}\end{cases} \quad (23)$$

where x is the displacement of the bar end, y the displacement of the transducer, f_b and f_t indicate the forces which act respectively on the bar and on the transducer, $\mu=\frac{m_t}{m_b}$, and Q_t and Q_b are the quality factor of the two oscillators. As it is well known, these two coupled oscillators have two vibrational normal modes, whose frequencies and merit factors $\nu_\pm$ and $Q_\pm$ can be determined experimentally with good accuracy.

The a.c. electrical voltage at the output of the transducer is proportional to the relative displacement of the transducer to the bar end:

$$\zeta(t)=y(t)-x(t)$$

Applying the Fourier transform to the above system of equations, we find

$$\tilde{\zeta}=\frac{1}{D}\left[\frac{\tilde{f}_b}{m_b}\omega^2+\frac{\tilde{f}_t}{m_t}(\omega_b^2-\omega^2+j\omega\frac{\omega_b}{Q_b})\right] \quad (24)$$

where $\tilde{x}$, $\tilde{y}$ and $\tilde{\zeta}$ are the Fourier transform of $x(t)$, $y(t)$ and $\zeta(t)$, and D the determinant of the system (23). Since $Q\approx 10^6$ and $\omega\approx\omega_b$ we express $\mid\tilde{\zeta}\mid$ using the angular frequencies $\omega_\pm$, that are directly measured quantities:

$$\mid\tilde{\zeta}_\pm\mid=\frac{|\tilde{g}_{eff}|}{|D|}=\frac{(\tilde{f}_b/m_b)\omega_\pm^2}{|D|}+\frac{(\tilde{f}_t/m_t)\omega_\pm^2}{|D|}\left(\frac{\omega_b^2}{\omega_\pm^2}-1\right) \quad (25)$$

where D is

$$D(\omega)=\left[\omega_+^2-\omega^2+\frac{i\omega_+\omega}{Q_+}\right]\cdot\left[\omega_-^2-\omega^2+\frac{i\omega_-\omega}{Q_-}\right]$$

This equation shows that, in the neighbourhood of each mode, the frequency response closely approximates that of a Lorentzian (second order) system. In fact, when the dynamical gravity field generator rotates with $\tilde{\omega}\simeq\frac{1}{2}\omega_+$ or $\tilde{\omega}\simeq\frac{1}{2}\omega_-$, the corresponding response of the mechanical system is expressed by (25). The steady state amplitude of the mechanical output signal, after a transient with time constant $\tau_\pm=2(Q_\pm/\omega_\pm)$, is therefore

$$\mid\tilde{\zeta}_\pm\mid\simeq\mid\tilde{g}_{eff}\mid\frac{\omega_\pm^2}{(\omega_\mp^2-\omega_\pm^2)[(\omega_\pm^2-\omega^2)^2+(\omega\omega_\pm/Q_\pm)^2]^{1/2}} \quad (26)$$

with $\omega=2\tilde{\omega}$, with very good approximation since $Q_\pm>>1$. The main contribution to $\mid\tilde{g}_{eff}\mid$ comes from $\frac{\tilde{f}_b}{m_b}$; from (16) we have

$$\left|\frac{\tilde{f}_b}{m_b}\right|=\left|\frac{G_0}{N}(\gamma_N+\gamma_Y)\right|. \quad (27)$$

The additional contribution due to $\tilde{f}_t$ is a small perturbation that we evaluate by representing the transducer as a point-like mass that oscillates in the x_3 direction of the reference frame introduced in Sect. 2. The perturbation term is computed in terms of the function $r(\delta)$, i.e.

$$(\tilde{f}_t/m_t)\left(\frac{\omega_b^2}{\omega_\pm^2}-1\right)=-\frac{3}{2}G_oM_q\mid r(\delta)\mid$$

that, under our assumption, is

$$\mid r(\delta)\mid=2N\left(\frac{\omega_b^2}{\omega_\pm^2}-1\right)\left\{\frac{1}{[\delta^2+L^2/4]^4}+\frac{25}{4}\cdot\frac{L^2/4}{[\delta^2+L^2/4]^5}+5\frac{L^2}{4}\frac{(L^2/4-3\delta^2)}{[\delta^2+L^2/4]^6}\right\}^{1/2} \quad (28)$$

The capacitive transducer, biased with a constant electric field E, converts the mechanical signal $\zeta(t)$ into an electrical one $V_t(t)$:

$$V_t = \gamma_t E \frac{C}{C + C_P} \zeta(t) \tag{29}$$

where γ_t is a transducer geometrical factor, C is the active capacitance of the transducer and C_P is its stray capacitance. This voltage is fed to a d.c. SQUID superconducting amplifier through an electric network that includes a superconducting transformer to match the high output impedence of the transducer to the low input impedance of the dc SQUID. The electromechanical transfer function W that links the relative displacement $\zeta(t)$ and the voltage at the SQUID output is

$$W(\omega) = A_{SQUID} \frac{1}{\mid Z(\omega) \mid} \gamma_t E \frac{C}{C + C_P}$$

where $Z(\omega)$ is the impedance of the RLC electrical circuit where the signal current generated by the transducer flows, and A_{SQUID} is the transfer function between this current and the output voltage of the SQUID. Here we note that the RLC circuit constitutes a third oscillator of electrical nature coupled to the two mechanical oscillators. The perturbation of the mode parameters $(Q_\pm, \omega_\pm)$ is weak, because the resonant frequency of this circuit is sufficiently higher, and can be neglected in first approximation. However, changes in the operating point of the SQUID, which are accompanied by variations of its input inductance, can cause very small variations of the mode frequencies ν_+ and ν_-. Due to the high Q values of the modes ($\simeq 10^6$), even frequency variations of a fraction of a mHz affect the response to a monochromatic excitation.

Finally, the r.m.s. value of the output voltage due to the monochromatic near field is

$$V_{r.m.s.\pm} = \frac{1}{\sqrt{2}} W_\pm \zeta_\pm \tag{30}$$

Thus, the detector output turns out to be a linear function of g_{eff}.

4 The rotor and its performances

The rotor was designed in collaboration with the Department of Mechanics of the Politecnico di Torino. The aim of this collaboration was to set up an experimental configuration in which a body with a large quadrupole moment can be safely spun up to a frequency range of $(450 \div 470)\ Hz$. It is obvious that the maximum diameter of the body is limited by the very high angular velocity requested. Moreover, as discussed in Sect. 1, a body with a large difference between the two principal moments of inertia in the rotation plane is needed in order to have a large quadrupole moment, but this condition is known to cause stability problems in specific ranges of the rotation frequency (supercritical regions [22,23].

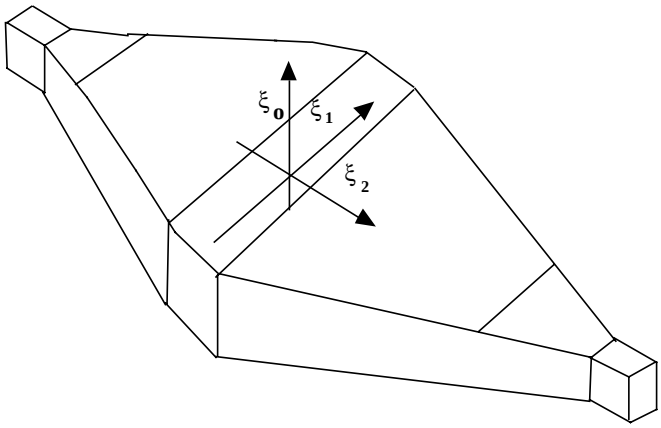

Fig. 2. Sketch of the rotor shape

In order to overcome this problem and to maximize the quadrupole moment, a nearly constant stress bar was carefully designed. The constant stress bar is a solid body whose cross section depends on the distance y from the rotation axis of the bar according to the law

$$S(y) = S_0 \exp\left(-\frac{\rho_r \omega^2 r_r}{2\sigma_r} \frac{y^2}{r_r^2}\right) \tag{31}$$

where ρ_r is the material mass density, σ_r the uniaxial design stress and r_r the maximum radial dimension of the body.

We chose an isotropic material, the aluminium alloy 2024, and, for a typical rotation frequency of 462 Hz and an applied uniaxial stress of $\simeq$ 230 MPa, that is consistent with the condition of safe operation, we obtained a maximum radius of $r_r \simeq 0.25\ m$ The actual shape of the rotor is shown in Fig. 2. Since the bar is highly stressed, a three-dimensional computer analysis was performed with Finite Elements Methods (FEM) in order to evaluate deviations from the theoretical constant stressing and to derive the main rotor characteristics.

The rotor itself was built by ElettroRava of Torino (Italy). It is a bar of 13.9 kg with a quadrupole moment $M_q = 6.65 \cdot 10^{-2}\ kgm^2$. The rotor driving system is an asynchronous electric motor and the rotation of the bar is monitored by means of an opto-electronic device. We drive the motor with an electric frequency which is slightly higher than the rotation frequency ($\simeq 1\ Hz$). As a consequence the main electromagnetic disturbance is 1 Hz far from our frequency band of interest. When the rotation frequency regime is achieved, the rotation signal provides the information required for controlling the motion of the rotor. This signal is compared with the square wave generated by the master synthesizer of the system (locked to a very stable Rb oscillator) whose frequency is set at one half of the resonance frequencies of the gravitational wave detector. The phase difference between the rotation signal and the synthesizer output is the error signal of a control system by means of which the rotor is phase-locked to the reference oscillator (see Fig. 3).

The electric motor and the bar are mounted in a stainless steel vacuum chamber. For safety reasons (the energy

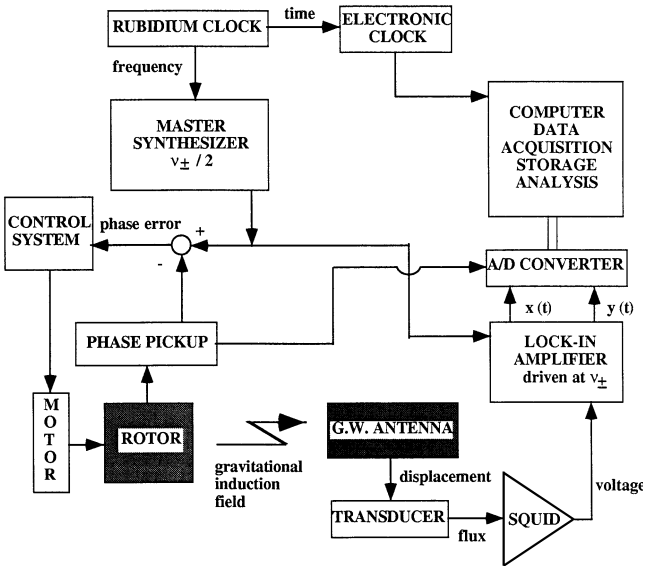

Fig. 3. Block diagram of the phase control of the system

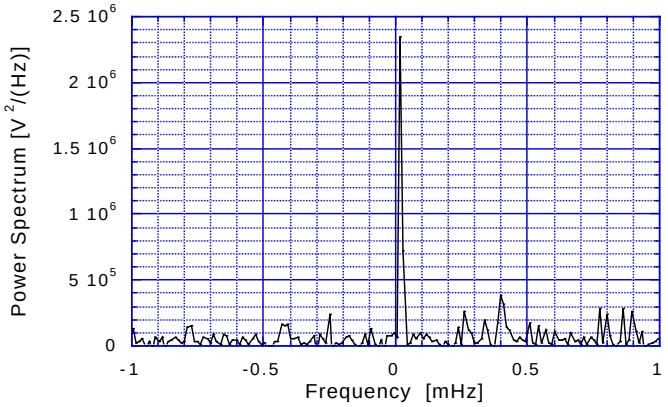

Fig. 4. Fast Fourier Transform of the opto signal of the rotor. The resolution of the spectrum is $24\,\mu Hz$

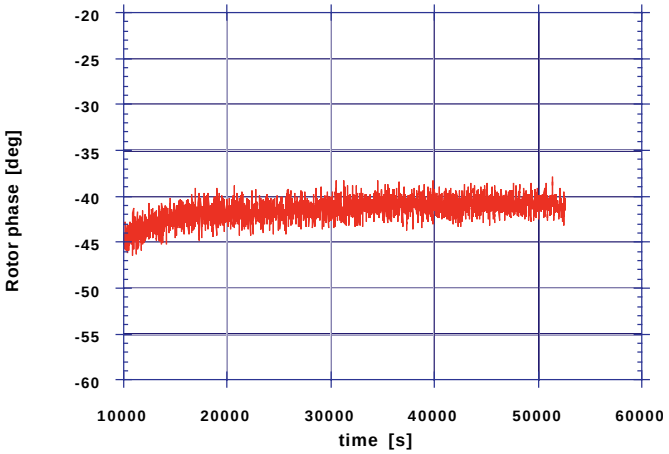

Fig. 5. The phase of the rotation signal Φ_R, measured with respect to the phase signal of the master synthesizer, versus time, during the same test run. The rotor was started at $t = 0$. In the diagram we report only the data after the rotor phase lock. The slow phase drift in the initial part of the curve is due to the fact that the rotor is approaching thermal equilibrium

stored in the rotor running at 460 Hz is $\simeq 0.6\ MJ$) the inner lateral wall of the vacuum chamber is protected with a steel ring 5 cm thick. On the rotation axis of the system, between the rotor and the driving system, a single stage of a turbo molecular pump is mounted which minimizes the pollution of the vacuum zone where the rotor spins, due to the lubrication fluid. Before starting the spinning of the bar the chamber is evacuated by means of a rotary pump and, when the rotation frequency is in the range of 460 Hz, the turbo molecular stage insures a vacuum of $1 \cdot 10^{-4}$ Pa.

We measured the residual vibrations of the system by means of a Bruel Kjaer model 4370 accelerometer. The typical values measured on the top of the vacuum chamber are 1.4 ms^{-2} at the rotation frequency and $4 \cdot 10^{-2}\ ms^{-2}$ at the detection frequency (twice the rotation frequency).

In order to reduce the e.m. and acoustic disturbances generated by the rotor, we built an auxiliary shield: a cubic box with a volume of 1 m^3 that encloses the whole system. The shield is made of pure aluminum, 5 mm thick, and its inner walls are completely covered by a material acting as an acoustic absorber. All the system stands on a bogie that can be moved, along two rails, in a direction perpendicular to the antenna axis.

The spin-up time of the rotor to the final frequency of 460 Hz is of the order of 20 minutes. When the feedback control is operating, after an initial transient of few seconds, the rotor spins exactly at the frequency of the master synthesizer. The phase stability is influenced by several factors and, in particular, it turns out to be sensitive to power line disturbances. Moreover, the electric motor requires a water refrigeration system, and we observed that the phase stability is improved when, after the rotor spin-up, the equilibrium temperature of the system is reached; this requires a time of the order of two hours.

The performance of the rotor system, in particular its phase and frequency purity, were finally checked experimentally. We drove the rotor at the frequency of 453 Hz, that is close to one half of the resonance frequencies of the modes.

A square wave obtained from the rotation signal was sent to a lock-in amplifier driven by the master synthesizer. The lock-in output, sampled at 1 s for 10 hours, was recorded on magnetic tape and analysed off-line. In Fig. 4, we show the Fast Fourier Transform (FFT) of this signal obtained with all the data of this run. We notice that the peak lies in just one bin of the discrete spectrum, thus defining an upper limit of 24 μHz (corresponding to the reciprocal of the observation time) for the spectral width of the rotor signal. In Fig. 5, we show the corresponding time evolution of the phase of the rotation signal Φ_R, measured with respect to the phase of the master synthesizer, measured during in the same test run. Finally we carefully analyzed the statistical properties of the phase fluctuation of the rotor. The histogram of the Fig. 6, performed with the same data, shows a gaussian behaviour of Φ_R with a standard deviation of 6^o.

Table 1. Parameters of the experimental apparatus for the two runs

	First run	*Second run*
Quadrupolar moment, M_q	$6.65 \cdot 10^{-2}\ kgm^2$	$6.65 \cdot 10^{-2}\ kgm^2$
Rotor mass, M_r	$13.9\ kg$	$13.9\ kg$
Detector mass, $2m_a$	$2270\ kg$	$2270\ kg$
Detector length, L	$2.9722 \pm 0.0001\ m$	$2.9722 \pm 0.0001\ m$
Detector radius, R	$0.3033 \pm 0.0001\ m$	$0.3033 \pm 0.0001\ m$
Frequency of the first normal mode, ν_-	$911.270240\ Hz \pm 15\ \mu Hz$	$907.501625\ Hz \pm 15\ \mu Hz$
Frequency of the second normal mode, ν_+	$937.060\ Hz \pm 1\ mHz$	$923.724290\ Hz \pm 15\ \mu Hz$
Quality factor of ν_-, Q_-	$(1.099 \pm 0.003) \cdot 10^6$	
Quality factor of ν_+, Q_+		$(5.572 \pm 0.006) \cdot 10^6$
Decay time of ν_-, τ_-	$(384 \pm 1)\ s$	
Decay time of ν_+, τ_+		$(1920 \pm 2)\ s$
Fundamental frequency of the antenna, ν_b	$913.04\ Hz$	$916.54\ Hz$
Transducer gap,d	$36\ \mu m$	$65\ \mu m$
Transducer effective mass, m_t	$0.146\ kg$	$0.340\ kg$
Transducer geometrical factor, γ_t	0.73	0.89

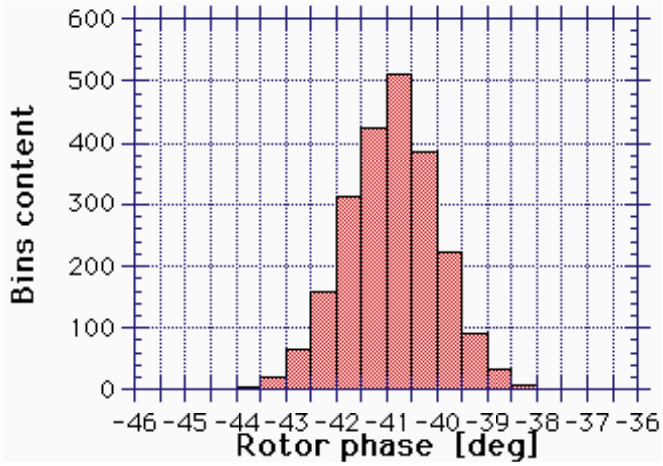

Fig. 6. Histogram of the rotor phase measurements after achieving thermal equilibrium

5 The cryogenic detector

A detailed description of the gravitational wave antenna of the Rome group (Explorer) installed at the CERN laboratory in Geneva has been given in previous papers [19, 20]. We recall here some basic informations on the experimental apparatus.

The antenna is a cylindrical bar (60 cm in diameter and 297 cm in length) of Al 5056 with mass M=2270 kg and reduced mass $m_b = M/2$ for the fundamental longitudinal vibrational mode ($\nu_b \simeq 916$ Hz at the liquid helium temperature). The antenna is located inside the vacuum enclosure of a liquid helium cryostat and is suspended with a Titanium alloy cable wrapped around the circular section containing the center of gravity. The Titanium cable constitutes the first of a multiple stage system designed to filter external mechanical disturbances, which provides 220 dB of attenuation at 900 Hz.

The resonant capacitive transducer is located at one end of the bar. Its resonating part has the shape of a mushroom which vibrates in its lowest symmetric flexural mode with reduced mass m_t.

We performed two separate run of measurements, with the Explorer antenna equipped with two different transducers. In the first run the transducer had $m_t = 0.15$ kg and the gap between the plates of the transducer capacitor was $d = 36\ \ \mu$m. In the second run the transducer was changed in order to reduce its electric and acoustic losses. In the new configuration the vibrating plate was heavier, $m_t = 0.34$ kg, and the gap larger $d = 63\ \ \mu$m. In both cases the bias electrical field of the transducer could be adjusted up to 8×10^6 V/m by means of an external battery. (We recall that the transducer frequency ν_t depends on the electrical field in the gap, thereby affecting the frequencies of the modes $\nu_\pm$.)

In both the runs we biased the transducer at 23 V one day before starting the measurements. This was done in order to reduce the effects due to the relaxation processes of the dielectric polarization in the decoupling capacitor. During all the measurements we maintained the transducer connected to the battery through a 10 GΩ resistor. A summary of all the parameters of the system is given in Table 1.

The electrical output of the transducer is applied to the SQUID amplifier through a decoupling capacitor C_d and an air core superconducting transformer that provides the required impedance matching between the transducer and the low input impedance of the amplifier. Since the SQUID gain depends on the actual operating point of the device, it is continuously monitored by sending a sine wave signal to the SQUID, through an auiliary coil, at a frequency ν_{cal}. As shown in Fig. 7, the output signal from the amplifier V(t) is sent to lock-in amplifiers which demodulate it at the mode frequencies (ν_+, ν_-, ν_{cal}). The outputs of the various lock-in amplifiers (V_-, V_+, V_{cal}) are sampled at time intervals of $\Delta t = 0.290$ s, processed by a 12 bit analog to digital converter and sent to a VAX 3800 computer for real time analysis and recording on the computer memory. We also record the Universal Time, provided by

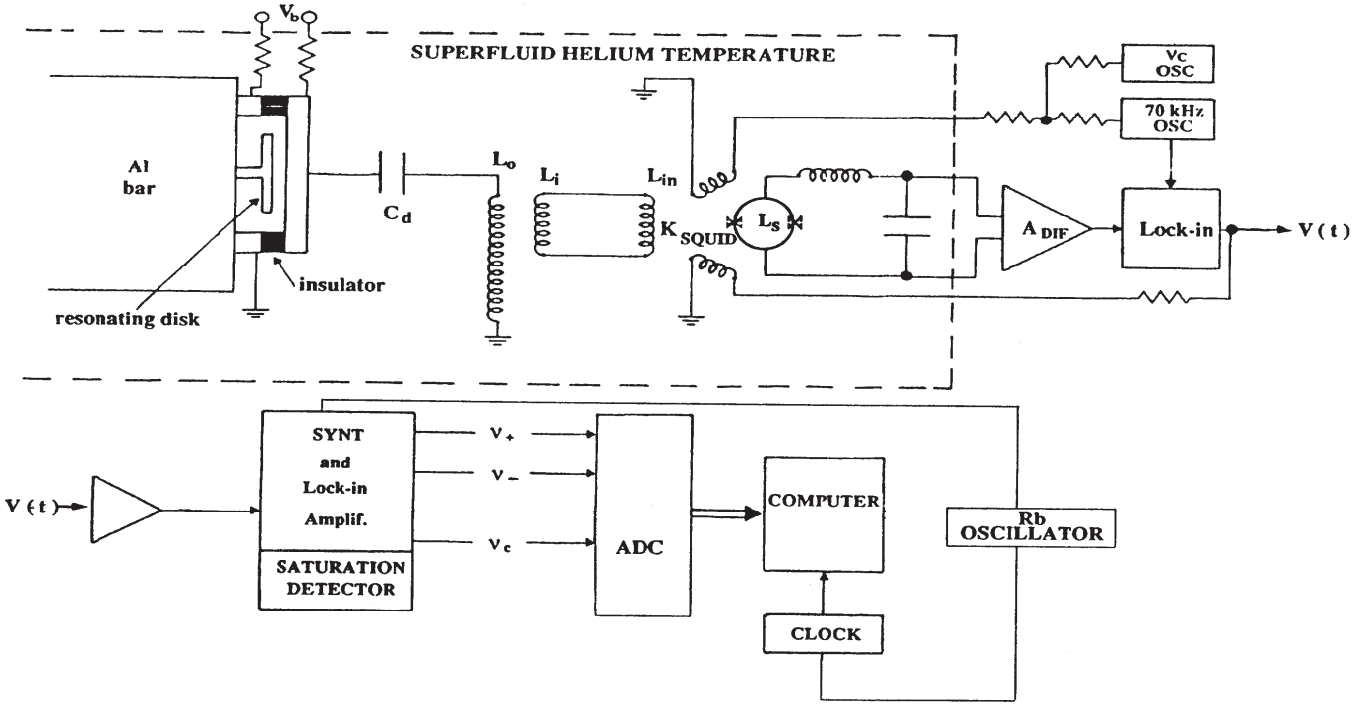

Fig. 7. Scheme of the gravitational wave detector. The part in the dashed section is cooled at low temperatures

a combination of a radio clock and a Rb frequency standard. The Rb oscillator also provides a stable reference to all synthesizers that drive the lock-in amplifiers.

The detector noise is due to two different stochastic processes: the wide band noise of the electronic amplifier and the narrow band thermal noise of the detector (the Brownian motion of the mechanical oscillators). The wide band electronic noise is basically uncorrelated and its contribution to the output noise can be made negligible by integrating the data for 1 second. The correlation times of the thermal fluctuations of the $\nu_{\pm}$ modes are the time constants $\tau_{\pm} = 2Q_{\pm}/\omega_{\pm}$. Therefore, in principle, to reduce this noise contribution we should integrate for times much longer than $\tau_{\pm}$. However this is not needed, because the signal generated by the gravitational interaction, with the transducer biased at 23 volt, with data integration time of 1 s, and with the rotor set at a distance $\delta \simeq 2$ m, is about 500 times larger than the intrinsic noise of the antenna.

The experimental apparatus of Explorer includes a vibration sensor (the same model of accelerometer used on the rotor), and a magnetic field sensor (search coil), both located on the cryostat. These sensors monitor the environment of the laboratory and are used to make sure that external noise produces effects on the antenna output well below the Explorer intrinsic noise.

During the measurements, in addition to the VAX system, we also used a smaller data acquisition system based on a analog to digital converter controlled by an Apple personal computer with a lower acquisition rate (10 s). This system was used to record the outputs of the lock-in driven at the antenna mode excited by the rotor and the outputs of the lock-in used to monitor the phase and the amplitude of the rotation signal of the rotor. In this way, we can relate the phase fluctuations of the antenna output to the phase fluctuations of the rotor.

6 Study of the systematic effects

The antenna response to the sinusoidal excitation induced by the rotor depends critically both on the merit factor of the excited mode and on the detuning of the driving frequency with respect to the resonance frequency of the mode. In particular the high Q value of the antenna corresponds to a very narrow width of the resonance ($\simeq 830\mu$Hz): this implies that the resonance frequencies should be known within a few tens of μHz. We have shown in the previous section the monochromatic purity of the signal and its phase stability, here we discuss the limits on the frequency stability of the detector.

The stability of the mode eigenfrequencies depends, indeed, on several effects. Beside a very small temperature effect, they can drift due to slow changes of the bias voltage of the transducer, and to changes of the operating point of the SQUID, which, due to the non-linear nature of this device, induce variations of its input inductance. The temperature effect is negligible because the bar temperature is very stable: $2.14 \pm 0.05K$. This is obtained by maintaining the vacuum chamber, where the detector is located, completely surrounded by liquid helium in superfluid regime. As regards the variations of the transducer bias voltage, the measurements were performed at 23 V, i.e. a value one order of magnitude smaller than usual, thereby strongly reducing both the dependence of the mode frequency on this voltage and the coupling be-

tween the mechanical oscillators and the readout electric circuit. In fact, in the case of detection of signal bursts, a high bias voltage is required in order to optimize the signal to noise ratio of the detector, while for monochromatic excitations this condition is irrelevant. The voltage stability of the battery, used to bias the transducer, was monitored as a function of the room temperature obtaining a typical value 2.8 10^{-3} V/^{o}C. This weak dependence, together with the low value of the transducer bias voltage, implies that the thermal drift of the battery voltage do not produce any detectable variation of the $\nu_{\pm}$ frequencies.

Finally, the frequency stability of the antenna resonances was experimentally verified. At the beginning and at the end of each measurement run, the frequency of the detector mode ν_{-} (chosen for the experiment in the first run) was carefully measured by exciting the mode, with a small piezoelectric ceramic glued on the antenna, and observing the free decay of the antenna signal through the lock-in driven at ν_{-}. In particular, by measuring the phase of the free decay signal we are able to conclude that the mode frequency $\nu_{-} = 911.270240 \pm 1.5 \cdot 10^{-5}$ Hz was stable within 15 μHz during all the measurements. From the amplitude measurements of the free decay of the mode which was repeated systematically during the run, we derived the decay time $\tau_{-} = 384 \pm 1$ s and the quality factor $Q_{-} = (1.099 \pm 0.003)$ 10^6.

We applied the same method during the second run. This time, we analyzed data taken by forcing the detector at the higher vibrational mode $\nu_{+} = 923.724290 \pm 1.5 \cdot 10^{-5}$ Hz and we measured several times during the run $\tau_{+} = 1920 \pm 2$ s corresponding to $Q_{+} = (5.572 \pm 0.006) \cdot 10^6$. Also in this case the frequency stability of the detector is about 15 μHz, but it has to be compared with a mode bandwidth a factor 5.5 narrower than that of the previous run.

We also considered the possible effects of the acoustic and electromagnetic disturbances produced by the rotor, the motor and the associated instrumentation. We performed tests by driving at the $\nu_{\pm}$ frequency a mechanical vibrator, mechanically coupled to the external vacuum tank of Explorer, and monitoring its effects by means of several accelerometers, including one inside the Explorer vacuum shell. The amplitude of the driving force of the vibrator was gradually increased until the corresponding antenna response at $\nu_{\pm}$ became observable.

From these measurements we were able to estimate the overall acoustic transmission of the cryostat and the antenna suspension system at the $\nu_{\pm}$ modes, obtaining a total amplitude attenuation of 220 dB (10^{-11}).

The acoustic effect of the rotor was investigated by spinning it at a frequency ν_R slightly different from one half of that of the $\nu_{\pm}$ modes ($2\ \nu_R - \nu_{\pm} \simeq 1$ Hz). In this condition we detected no increase of the antenna output noise level at $2\nu_R$, while the acceleration measured by the auxiliary accelerometer of Explorer was $\simeq 3$ 10^{-4} ms^{-2} and it was independent from ν_R. This acceleration was also measured for various distances δ between the rotor and the antenna, observing a decrease of a factor two in the amplitude with δ increasing from 1.9 m to 3.5 m. Taking into the account the acoustic transmission of the system, we conclude that the acoustic disturbance of the rotor at $\nu_{\pm}$ corresponds to an equivalent acceleration of the antenna two order of magnitudes lower than that of the gravitational near field generator.

Moreover, the e.m. background generated by the rotor was carefully analysed. The main e.m. disturbance is at the frequency of the electric signal driving the motor, which is 1 Hz higher than the rotation frequency and it is not a source of concern. Nevertheless, we measured the e.m. attenuation of the system and the e.m. background generated by the rotor at $\nu_{\pm}$ using the search coil of Explorer. In this case too we performed "active" tests using an external coil to produce a variable magnetic field at $\nu_{\pm}$. From the results of the above tests we conclude that the upper limit for the e.m. background is 2 10^{-4} of the gravitational signal at a distance of about 2 m.

7 Experimental results

The cryogenic antenna was excited several times by the dynamic field generated by the rotor for various values of the distance δ between the generator and the detector. The position of the rotor with respect to the antenna center was measured in two steps. During a stop run of the Explorer detector, when we had access inside the cryostat, we measured the antenna orientation and the antenna center coordinates with respect to a reference system external to the cryostat. The different values of δ, used in the various measurements runs, were measured with respect to this reference system when the Explorer was in operation with the antenna at 2 K. We expect that, while cooling from room temperature to the final low temperature, the positions of the inner containers of the cryostat may change. This is the main source of error on the definition of the antenna center, that we estimate to be of the order of ± 1 mm.

Once the rotor phase is locked at the chosen mode frequency, it is possible to obtain from the two output $x(t)$ and $y(t)$ of the lock-in both the amplitude $V = \sqrt{x^2 + y^2}$ and the phase $\Phi_D = \arctan(y/x)$ of the oscillations of the antenna relative to the master synthesizer.

At the beginning of each run we carefully measured the resonance frequency of the $\nu_{\pm}$ mode and, once the rotor was running near $\nu_{\pm}/2$ with a relatively stable phase, we closed the control loop driven by the master synthesizer. We then observed the exponential growth of the antenna signal. After a time of the order of $3\tau_{\pm}$ the signal reached a steady state vibration amplitude. We use this value to compare the experimental observations to the theoretical predictions.

7.1 The first run of data taking

The first run of measurements was carried out by exciting the ν_{-} antenna mode.

For each position of the rotor (see Table 2) we recorded amplitude and phase of the output signal and we com-

Table 2. Data of the first run

$\delta \pm 5 \cdot 10^{-4}$ (m)	$V(\delta)$ (mV)	$\Delta V_{tot}(\delta)$ (mV)
1.9170	128.4	2.0
2.4680	56.1	2.0
2.9660	25.0	2.0
3.4670	13.1	2.0

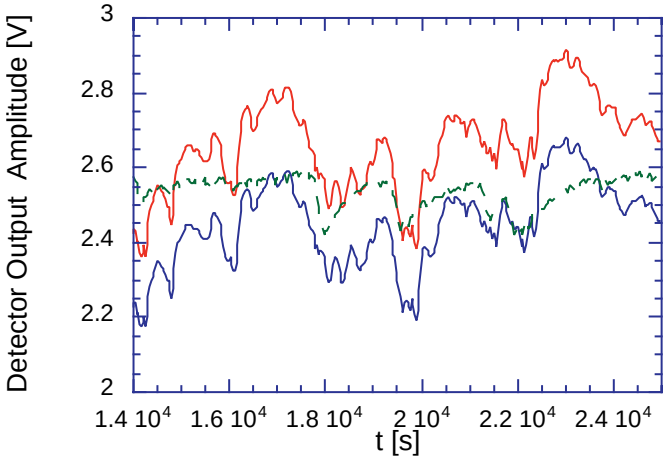

Fig. 8. Amplitude of the output signal of Explorer with the rotor set at a distance $\delta = 1.9710\ m$ and turning at $\nu_-/2$ (marked lines). The two continuous lines are the $\pm 1\sigma$ theoretical curves, computed as described in Appendix 1

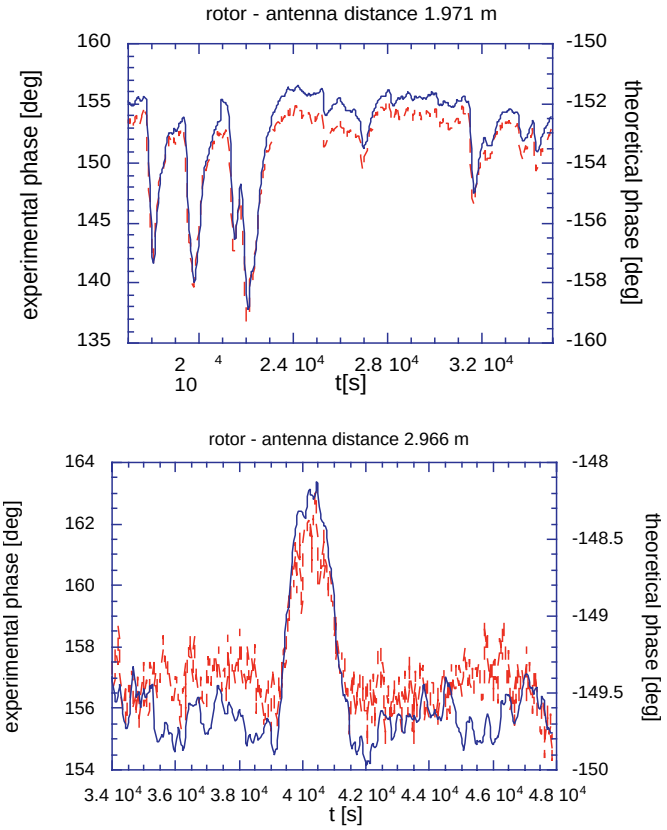

Fig. 9. a Comparison between the theoretical phase (continuous line) and the measured phase (marked line), for a distance $\delta = 1.9170\ m$, **b** Comparison between the theoretical phase (continuous line) and the measured phase (marked line), for a distance $\delta = 2.9660\ m$

puted the mean values of the amplitude over periods of the order of one time constant: during this span of time a good phase stability of both the rotor and the detector was observed. With this technique we can decrease the statistical error on the amplitude measurements, even if, to obtain a value with a lower statistical error we should use all the data taken during long periods of resonant excitation.

We experimentally verified that large changes of the rotor phase determine, with a delay of the order of τ_-, significant variations of the phase as well as of the amplitude of the output signal.

We inferred that the amplitude changes of the output signal observed over long periods ($\simeq$ 10 hour) were mainly due to the residual phase fluctuations of the rotor. We checked this statement by computing the output signal using the data of the rotor phase Φ_R taken during the same period of time. This was done performing the numerical integration of the final expressions reported in the Appendix 1 and 2. In Figs. 8 and 9 we notice the good agreement between the real data and the results of the numerical computation.

7.2 The second run of data taking

The second run of data taking was performed several months later, after an antenna warm-up that allowed us to open the Explorer cryostat and install a new transducer, with better performance.

The new transducer had larger effective mass and larger gap: this implied that the mode frequencies changed to new values, but their dependence on the transducer field was somewhat weaker.

Moreover, the new transducer had lower mechanical and electric dissipations, thereby providing Q values of the modes about five times larger than in the previous run. The most important consequence is that the steady state signal response to a resonant excitation is increased by the same factor, with a corresponding improvement on the relative statistical error of our measurements. Higher Q values, however, provide no improvement with respect to the systematic effects due to the coherent acoustic and e.m. excitation of the detector modes.

However, in the new experimental configuration it was possible to increase the rotor distance up to 5.9 m, while, in the first run, data had been taken for a range $1.9 < \delta < 3.5$ m. The procedure followed in this second run is similar to the previous one. The transducer was biased again at -23 V, now corresponding to a lower electric field because of the larger gap. We performed measurements exciting both modes, but we shall only report the results obtained at ν_+ since during the excitation at ν_-, the phase stability of the rotor and the frequency stability of the detector were not satisfactory.

Table 3. Data of the second run

$\delta \pm 5 \cdot 10^{-4} (m)$	$V(\delta)$ (mV)	$\Delta V_{tot}(\delta)$ (mV)
1.9170	690.3	4.5
3.2290	110.4	4.4
3.7229	50.3	4.5
4.2241	27.3	4.4
4.7250	16.6	4.6
5.0264	11.9	4.4
5.2261	8.2	4.4
5.9710	2.0	4.5

Also in this case the first data taking was done with the rotor at a distance $\delta = 1.971$ m from the centre of the antenna. We checked again the frequency response of the detector by performing three measurements near the resonance peak. Then we excited the antenna by spinning for one night the rotor at half the resonance frequency ν_+. During the data taking with the rotor located in the other distances we checked only the frequency stability by observing the phase of the output signal during a free decay. The results of the measurements are reported in Table 2. We notice that in this data set the difference between the phase of the output signal and twice the rotor phase is not as stable as in the first run and that it changes when the distance is increased. This is a consequence of the residual acoustic coupling between the rotor and the detector: it becomes more relevant at larger distances because the response to the gravitational signal decreases more rapidly.

8 The data analysis procedure

As discussed in the previous section, with a longer data taking and with a suitable data analysis we can reduce the statistical error by at least one order of magnitude. However, in order to derive the upper limit curve $\alpha(\lambda)$ we have to take into the account also the systematic errors $(\Delta V/V)_{syst}$ due to the coherent excitation of the residual acoustic and e.m. signal. The main contribution to $(\Delta V/V)_{syst}$ is due to the residual acoustic transmission of the cryostat. Using the results of the acoustic transmission tests described in Sect. 6, we have estimated $(\Delta V/V)_{syst}$ in the previous section.

The data analysis is based on a standard χ^2 fit, in which the theoretical excitation and the experimental values are compared. Since the experimental data are taken in two runs of different experimental conditions, we define a χ^2 function as the sum of two terms one for each group of data:

$$\chi^2 = \sum_{j=1}^{4} \frac{(x_j - y_j(\mathbf{\Lambda}))^2}{\Delta x_j^2} + \sum_{i=1}^{8} \frac{(x_i - y_i(\mathbf{\Lambda}))^2}{\Delta x_i^2} \qquad (32)$$

where x and Δx are the data and the corresponding errors. y is the theoretical function, and the multi dimensional vector $\mathbf{\Lambda}$ represents, through its components, the parameters characterizing the theoretical behaviour. In this case we deal with a three-dimensional parameters space: the coupling constant α and the two parameters N_1 and N_2, which are introduced to match the theoretical displacement function to the output voltage of the detector. The explicit expression of χ^2 is given below in terms of the F_N and F_Y integrals and of the $r(\delta)$ term:

$$\chi^2 = \sum_{j=1}^{4} \frac{\left[V_j - \frac{1}{N_1}\left(F_N(\delta_j) + \alpha F_Y(\delta_j, \lambda) + r(\delta_j)\right)\right]^2}{\Delta V_{tot\ j}^2} + \sum_{i=1}^{8} \frac{\left[V_i - \frac{1}{N_2}\left(F_N(\delta_i) + \alpha F_Y(\delta_i, \lambda) + r(\delta_i)\right)\right]^2}{\Delta V_{tot\ i}^2} \qquad (33)$$

The minimization of the (33) was performed by using MINUIT, the routine of the CERN software library [24]. We found the minimum value of α for each fixed value of λ in order to obtain the $\alpha(\lambda)$ dependence. We explored the range of λ from 0.3 m to 11.0 m, improving the step accuracy of λ in the range $1 \leq \lambda \leq 2.5$ m, around the minimum of the $\alpha(\lambda)$ function, and in the range $0.3 \leq \lambda \leq 1$ m to study the trend at shorter distances.

The minimization results slightly depend on the initial values assigned to the parameters. We assumed as initial values of N_1 and N_2 those obtained by minimizing the χ^2 function in the case of a purely Newtonian field ($\alpha = 0$). Concerning the initial value of α, we started the minimization using the result of the Ogawa [18] experiment, $\alpha \simeq 10^{-2}$. From the minimization procedure we also obtained the two standard deviation errors ($2\ \sigma_\alpha$). In this way we managed to produce a final curve compatible with those of the Gibbons and Whiting (GW) diagram [15].

9 Discussion of the results and conclusions

The results of the minimization procedure, i.e. the estimates of α vs. λ, are reported in Table 4. We notice that for no value of λ we have a corresponding α larger than its standard deviation σ_α. We conclude that we did not detect any Yukawian deviation of the Newtonian behaviour of the gravity interaction.

The upper limit on $\alpha(\lambda)$ is set by the corresponding error values. The upper limit function $2\sigma_\alpha(\lambda)$ is shown in Fig. 9. We notice that the minimum of this curve is:

$$2\sigma_\alpha < 2 \cdot 10^{-2} \quad for\ \lambda = 2.0\ m \qquad (34)$$

that sets our best upper limit for a Yukawian deviation superposed to the Newtonian field.

This limit, obtained by testing the Newtonian law in the distance range from 2 to 6 m and in the frequency range of 900 Hz, could be improved by modifying the present experimental set-up. The main changes would involve the acoustic filters and the e.m. shielding of Explorer that determine the systematic error of the gravitational measurements. However, a radical approach to the reduction of these effects, will have to wait for a stop run of the gravitational wave antenna, in order to assemble new seismo-acoustic filters inside the cryostat.

Table 4. Values of the coupling parameter α and its error $2\sigma_\alpha$ as a function of λ

λ (m)	α	$2\sigma_\alpha$
0.3	0.022	1.9
0.4	0.0077	0.44
0.5	0.0053	0.19
0.6	0.0041	0.11
0.7	0.0036	0.074
0.8	0.0034	0.057
1.0	0.0032	0.040
1.2	0.0032	0.033
1.3	0.0032	0.031
1.5	0.0033	0.028
1.8	0.0034	0.026
1.9	0.0035	0.026
2.0	0.0036	0.026
2.05	0.0036	0.026
2.1	0.0036	0.026
2.2	0.0037	0.026
2.3	0.0038	0.026
2.4	0.0039	0.026
2.5	0.0039	0.026
3.0	0.0044	0.027
3.5	0.0048	0.028
4.0	0.0053	0.030
4.5	0.0056	0.032
5.0	0.0060	0.034
5.5	0.0067	0.037
6.0	0.0072	0.040
6.5	0.0077	0.042
7.0	0.0082	0.045
7.5	0.0087	0.048
8.0	0.0092	0.052
8.5	0.0097	0.055
9.0	0.010	0.058
9.5	0.011	0.062
10.0	0.011	0.066
11.0	0.012	0.075

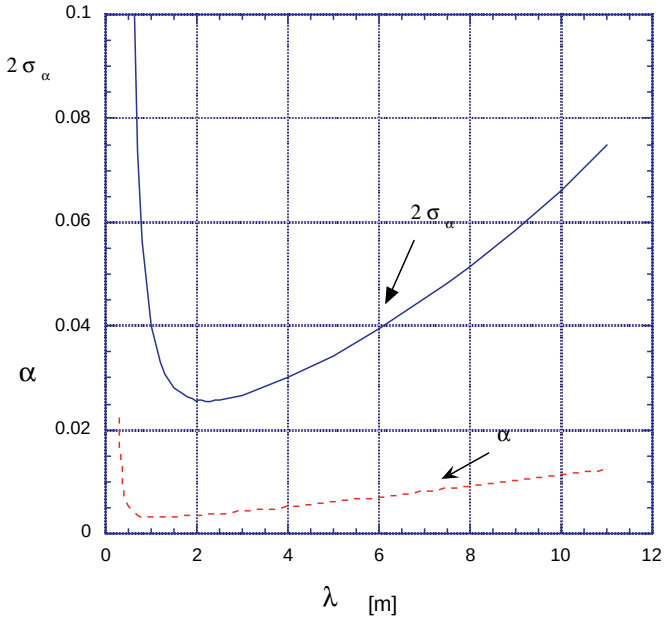

Fig. 10. Results of the minimization procedure. The dashed line represents α versus λ. The full line is the upper limit function of α obtained by plotting $2\sigma_\alpha$ versus λ. We notice that the $\alpha(\lambda)$ curve lies below the one of its corresponding error $2\sigma_\alpha$

Appendix 1

Influence of the forcing phase fluctuations on the antenna oscillations

The rotor phase $\gamma(t)$ was measured, as described in the paragraph 7.1, with an integration time of 30 seconds. In order to extract information concerning the amplitude of the forcing term due to the gravitational acceleration, we derive a dimensionless expression that depends on $\gamma(t)$ because we are just interested to the behaviour of the modulus of the forcing term. This function will be used to convert the integrated output data of the detector; this procedure allows us to compensate the effect of the phase fluctuations of the rotor.

Let us consider a damped harmonic oscillator subjected to a harmonic acceleration whose amplitude a_0 is constant and whose phase is changing with the time:

$$a(t) = a_0 e^{i(\alpha(t)+\omega t)} \tag{35}$$

The equation of motion for the harmonic oscillator will be:

$$\ddot{x} + \frac{\omega_0}{Q_0}\dot{x} + {\omega_0}^2 x = a_0 e^{i(\alpha(t)+\omega t)} \tag{36}$$

The forcing phase is the sum of two terms: an oscillating term at the rotation frequency ω, and a function $\gamma(t)$, whose analytical expression is unknown. $\gamma(t)$ was measured by integrating its value on a characteristic time of 30 seconds for all the run of data taking.

We look for a solution of the position variable $x(t)$ of the form

$$x(t) = m(t) x_0 e^{i(\phi(t)+\omega t)} \tag{37}$$

where $x_0 m(t)$ is the amplitude, equal to the product of the dimensionless and time dependent term $m(t)$ and of the constant term x_0 (with dimensions of a length):

$$x_0 = a_0 \frac{Q_0}{\omega\omega_0} \tag{38}$$

Substituting the expressions (35) and (37) into (36), and using the expression (38), we can write the harmonic oscillator equation in a form independent of a_0.

$$\ddot{y}(t) + \frac{\omega_0}{Q_0}\dot{y}(t) + \omega_0^2 y(t) = a'(t) \tag{39}$$

where $y(t) = m(t)e^{i(\phi(t)+\omega t)}$ and $a'(t) = e^{i\omega t + i\gamma(t)}$ are two dimensionless functions independent of a_0. The (39) is easily solved in Fourier space:

$$\tilde{y}(p) = \frac{\tilde{a}'(p)}{-p^2 + ip\frac{\omega_0}{Q_0} + \omega_0^2} \tag{40}$$

$\tilde{a}'(p)$ is derived performing the Complex Fast Fourier Transform (FFT) of the available data of the rotor phase,

and $\tilde{y}(p)$ is is obtained by computing numerically the complex ratio (40). Finally, by performing the inverse Complex FFT of $\tilde{y}(p)$, we derive the function $y(t)$.

Appendix 2

The antenna oscillations phase as a function of the forcing phase

To solve 39 we apply the Green function method, obtaining

$$y(t) = \frac{1}{\omega_0}\int_{-\infty}^{t} dt'\ e^{i(\omega t' + \gamma(t'))} e^{-\frac{(t-t')}{\tau}} \sin\omega_0(t-t') \quad (41)$$

Since $\gamma(t) \ll 1$ we approximate $e^{i\gamma(t)} \simeq 1 + i\gamma(t)$ and, using standard trigonometric relations we obtain:

$$\begin{aligned} y(t) \simeq\ & \frac{\tau}{2\omega_0}\sin\omega_0 t + \frac{1}{\omega_0}e^{-t/\tau}\left[\cos\omega_0 t\int_{-\infty}^{t} dt'\ \gamma(t')e^{t'/\tau}\right. \\ & \times \sin^2\omega_0 t' - \sin\omega_0 t\int_{-\infty}^{t} dt'\ \gamma(t')e^{t'/\tau} \\ & \left.\times \sin\omega_0 t'\cos\omega_0 t'\right] + i\left\{-\frac{\tau}{2\omega_0}\cos\omega_0 t\right. \\ & + \frac{1}{\omega_0}e^{-t/\tau}\left[\sin\omega_0 t\int_{-\infty}^{t} dt'\ \gamma(t')e^{t'/\tau}\cos^2\omega_0 t'\right. \\ & \left.\left. - \cos\omega_0 t\int_{-\infty}^{t} dt'\ \gamma(t')e^{t'/\tau}\sin\omega_0 t'\cos\omega_0 t'\right]\right\} \quad (42) \end{aligned}$$

where we have assumed $2\omega_0\tau \gg 1$ ($\omega_0\tau \approx 10^6 \div 10^7$).

We notice that the function $e^{t'/\tau}\gamma(t')$ changes slowly with time compared with the $\sin(\omega_0 t')$ term. Thus, the real and the imaginary part of the (42) become:

$$\begin{aligned} \Re y(t) \simeq\ & \frac{\tau}{2\omega_0}\sin\omega_0 t + \frac{1}{2\omega_0}e^{-t/\tau}\cos\omega_0 t\int_{-\infty}^{t} dt'\ \gamma(t')e^{t'/\tau} \\ \Im y(t) \simeq\ & -\frac{\tau}{2\omega_0}\cos\omega_0 t + \frac{1}{2\omega_0}e^{-t/\tau} \\ & \times \sin\omega_0 t\int_{-\infty}^{t} dt'\ \gamma(t')e^{t'/\tau} \quad (43) \end{aligned}$$

Defining the factor β as

$$\beta = \frac{e^{-t/\tau}}{\tau}\int_{-\infty}^{t} dt'\ \gamma(t')e^{t'/\tau} \quad (44)$$

we notice that $\beta \ll 1$ ($\tau \simeq 3\cdot 10^2$ and $\gamma(t) \ll 1$). Then we can rewrite the real and the imaginary part of $y(t)$ as:

$$\begin{aligned} \Re y(t) &= \frac{\tau}{\omega_0}\sin(\omega_0 t + \beta) \\ \Im y(t) &= -\frac{\tau}{\omega_0}\cos(\omega_0 t + \beta) \quad (45) \end{aligned}$$

Being

$$\phi(t) = \arctan\frac{\Im y(t)}{\Re y(t)} \quad (46)$$

we get the final expression of the antenna phase:

$$\phi(t) = \frac{\pi}{2} + \omega_0 t + \frac{e^{-t/\tau}}{\tau}\int_{-\infty}^{t} dt'\ \gamma(t')e^{t'/\tau} \quad (47)$$

Using the available data on $\gamma(t)$ and performing a numerical integration of (47) we derive the corresponding time evolution of the detector phase.

Acknowledgements. We express our thank to Mr. F. Bronzini, Mr. E. Serrani and Mr. R. Simonetti for their technical support and the survey group of the MT division of CERN for the measurements of the rotor position.

References

1. Fischbach E., Talmadge C., *Six years of the fifth force*, Nature **356**, 207–215 (1992); Fischbach E. et al., *Non newtonian gravity and new weak forces: an index of measurements and Theory*, Metrologia **29**, 213–260 (1992)
2. Chen Y.T., Cook A., *Gravitational experiments in the laboratory*, Cambridge University Press (1993)
3. Fujii Y., *Dilaton and possible non-newtonian gravity*, Nature Phys. Sci. **234**, 5–7 (1971); Fujii Y., *On the fifth force*, in Proceedings of the workshop on elementary particle picture of the universe, Ed. by Yoshimura M., Totsuka Y., Nakamura K. 207–218 (1987)
4. Fischbach E., Talmadge C., *The fifth force: an introduction to current research*, In 5th force neutrino physics, Proceedings of the XXIIIrd rencontre de Moriond, Gif sur Yvette, Edition Frontières 369–382 (1988)
5. Choen E.R., Taylor B.N., CODATA Bulletin **63**, 12 (1986)
6. Page T.L., *Radial velocities and masses of double Galaxies*, Astophys. J. **116**, 63–80 (1952)
7. Ohaniam H.C., Ruffini R., *Gravitation and Spacetime*, 2nd edition W.W. Norton and Company, New York (1994)
8. Rapp R.H., Geophys. Res. Lett. **14**, 730–732 (1987)
9. Eötvös R.v., Pekár D., Fekete E., Annalen der Physik (Leipzig) **68**, N.9, 11–66 (1922); Eötvös R.v., Pekár D., Fekete E., *Beiträge zum gesetze der proporzionalität von trägheit und gravität*, In Roland Eötvös Gerusammelte Arbeiten, Akadémiai Kiado, Budapest, 307–372 (1953)
10. Adelberger E.G. et al., *Testing the equivalence principle in the field of the Earth: particle physics at masses below 1 μeV*, Phys. Rev. **D 42**, 3267–3292 (1990); Adelberger E.G. et al., *Eötvös experiments, lunar ranging and the strong equivalence principle*, Nature **347**, 261–263 (1990)
11. Stacey F.D. et al., *Geophysics and the law of gravity*, Rev. of Mod. Phys. **59**, 157–174 (1987); Stacey F.D., Tuck G.J., *Geophysical evidence for non newtonian gravity*, Nature **292**, 230–232 (1981); Stacey F.D., Tuck G.J., Moore G.I., *Geophysical consideration in the fifth force controversy*, J. of Geophys. Res. **93, B9**, 10575–10587 (1988)
12. Zumberge M.A. et al., *Submarine measurement of the newtonian gravitational constant*, Phys. Rev. Lett. **67**, 3051–3054 (1991)
13. Speake C.C. et al., *Test of the inverse-square law of gravitation using the 300 m tower at Erie, Colorado*, Phys. Rev. Lett. **65**, 1967–1971 (1990)
14. Eckhardt D.H. et al, *Tower gravity experiment: evidence for non Newtonian gravity* , Phys. Rev. Lett. **60**, 2567–2570 (1988)

15. Gibbons G.W., Whiting B.F., *Newtonian gravity measurements impose costraints on unification theories*, Nature **291**, 636–638 (1981)
16. Sinsky J., Weber J., *New source for dynamical gravitational fields*, Phys. Rev. Lett. **18**, 795–797 (1967); Sinsky J., *Generation and detection of dynamic newtonian gravitational fields at 1660 cps*,Phys. Rev. **167**, 1145–1151 (1967)
17. Mio N., Tsubuono K., Hirakawa H., *Experimental test of the law of gravitation at small distances*, Phys. Rev. **D 36**, 2321–2326 (1987); Kuroda K., Hirakawa H., *Experimental test of the law of gravitation*, Phys. Rev. **D 32**, 342–346 (1985)
18. Ogawa Y., Tsubuono K., Hirakawa H. *Experimental test of the law of gravitation*, Phys. Rev. **D 62**, 729–734 (1982)
19. Bronzini et al., Cryogenics **25**, 234 (1985)
20. Astone P. et al., *Long–term operation of the Rome "Explorer" cryogenic gravitational wave detector*, Phys. Rev. **D 47**, 362–375 (1993)
21. Astone P. et al., *Evaluation and preliminary measurement of the interaction of a dynamical gravitational near field with a cryogenic gravitational wave antenna*, Zeit. Script C - Particles and Fields **50**, 21–29 (1991)
22. Crandal S.H., Brosen P.J. Jourmal of Applied Mechanics, **28**, 567 (1961)
23. Genta G., Journal of Sound and Vibrations, **124(1)**, 277 (1988)
24. CERN Program Library, *CERNLIB - Short Writeups*, Cern, Geneva, Switzerland (1996)